Cis-to-trans Isomerization of Spheroidene in the Triplet State as Detected by Time-Resolved Absorption Spectroscopy

Ritsuko Fujii,[†] Kentaro Furuichi,[†] Jian-Ping Zhang,[†] Hiroyoshi Nagae,[‡] Hideki Hashimoto,[§] and Yasushi Koyama*,[†]

Faculty of Science, Kwansei Gakuin University, Gakuen, Sanda 669-1337, Japan, Kobe City University of Foreign Studies, Gakuen-Higashimachi, Nishi-ku, Kobe 651-2187, Japan, and Department of Materials Science and Chemical Engineering, Faculty of Engineering, Shizuoka University, Johoku, Hamamatsu 432-8561, Japan

Received: April 9, 2001; In Final Form: October 9, 2001

Cis-to-trans isomerization upon excitation of the all-trans, 9′-cis, 13′-cis, 9-cis, 13-cis, and 15-cis isomers of spheroidene to the triplet state (by the use of anthracene as a sensitizer) was traced by submicrosecond time-resolved absorption spectroscopy. The time-resolved spectra were analyzed by means of singular-value decomposition and subsequent global fitting using a scheme having potential minima at the cis and trans positions in both the T_1 and S_0 states. The quantum yields of triplet-sensitized isomerization were also determined. The process of cis-to-trans isomerization in the T_1 state was clearly seen for the 13′-cis and 9-cis isomers. The quantum yield and the rate of cis-to-trans isomerization increased systematically in the order 13′-cis, 9-cis, 13-cis, and 15-cis T_1 species, whereas their rates of $T_1 \rightarrow S_0$ intersystem crossing were similar to one another and 6 times larger than that of the all-trans T_1 species. The $T_n \leftarrow T_1$ absorption maximum shifted to the blue in the above order, and reached to that of the all-trans T_1 species. Those observations were explained in terms of "the triplet-excited region" localized in the central part of the conjugated chain. A possible reason for the selection of the 15-cis configuration by a bacterial photoreaction center containing this carotenoid was discussed.

Introduction

Carotenoids (cars.) in the 15-cis configuration seem to be ubiquitously bound to the quinone-type and the iron sulfur-type reaction centers (RCs) (see ref 1 for a review). In the case of the quinone-type RCs, the 15-cis isomers of neurosporene, spheroidene, and spirilloxanthin were identified in the extracts from the RCs of *Rhodobacter* (*Rb.*) *sphaeroides* G1C,[2] *Rb. sphaeroides* 2.4.1,[3,4] and *Rhodospirillum rubrum* S1,[5] respectively. 15-*cis*-β-Carotene was found in the extract from the photosystem (PS) II RC of spinach.[6] In the iron sulfur-type RCs, on the other hand, 15-*cis*-γ-carotene and 15-*cis*-chlorobactene were identified in the extract from the RC of *Chlorobium tepidum*,[7] and 15-cis-β-carotene was found in the extract from the PSI RCs of both spinach[8] and *Synechococcus vulcanus*,[7] together with the all-trans isomers. (X-ray crystallography has identified 15-*cis*-spheroidene in the RC of *Rb. sphaeroides*[9−11] and 15-*cis*-1,2-dihydroneurosporene in the RC of *Rhodopseudomonas viridis*.[12] The cars. were modeled as the 13-cis isomers in a preliminary stage of X-ray analysis. X-ray crystallography of the PSI RC from *Synechococcus elongatus*, at 2.5 Å resolution, identified cis β-carotenes, which are now assigned to 9-cis, 13-cis, and di-cis isomers.[13] Contradictory reports have appeared, in addition to ours,[8] concerning the presence[14] and absence[15] of cis β-carotene(s) in the PSII RC. No X-ray structures have been published concerning β-carotene in this RC.)

Here, an interesting question to be addressed is what is the reason for the natural selection of the 15-cis configuration by the quinone-type bacterial RCs. In the RCs, an excess supply of light energy under the reducing conditions gives rise to reverse electron transfer and charge recombination at the special pair bacteriochlorophylls (BChl) to generate the triplet (T_1) state. The triplet energy needs to be transferred to one of the accessory BChls and then to the car. to be dissipated to avoid sensitized generation of singlet oxygen by triplet BChl[16−18](see ref 19 for a review). Because the car. and BChl molecules are in close contact in the RCs to facilitate efficient triplet-energy transfer, the most probable reason for the selection of the 15-cis configuration is its highest efficiency in dissipating the triplet energy.

To find out a unique property of the 15-cis configuration in the T_1 state, the all-trans, 7-cis, 9-cis, 13-cis, and 15-cis isomers of β-carotene, of which the structures are shown in Figure 1a, have been examined (see ref 20 for a review); time-resolved Raman[21] and electronic absorption[22] spectroscopies of the T_1 species that were generated from the set of cis−trans isomers lead us to the following conclusions: (a) As for the initial and the final ground-state configurations, excitation from and relaxation to the starting isomer took place for the all-trans isomer and the 7-cis and 9-cis (peripheral-cis) isomers, whereas excitation from the cis isomer and subsequent relaxation to the all-trans isomer was observed for the 13-cis and 15-cis (central-cis) isomers. (b) Upon triplet excitation, the all-trans and the 15-cis isomers showed the same Raman and electronic absorp-

* To whom correspondence should be addressed. Prof. Yasushi Koyama, Faculty of Science, Kwansei Gakuin University, 1-1-155 Uegahara, Nishinomiya 662-8501, Japan. Fax: +81-798-51-0914. Phone: +81-798-54-6389. E-mail: ykoyama@kwansei.ac.jp.

[†] Kwansei Gakuin University.

[‡] Kobe City University of Foreign Studies.

[§] Shizuoka University.

10.1021/jp011309n CCC: $22.00
Published on Web 02/14/2002

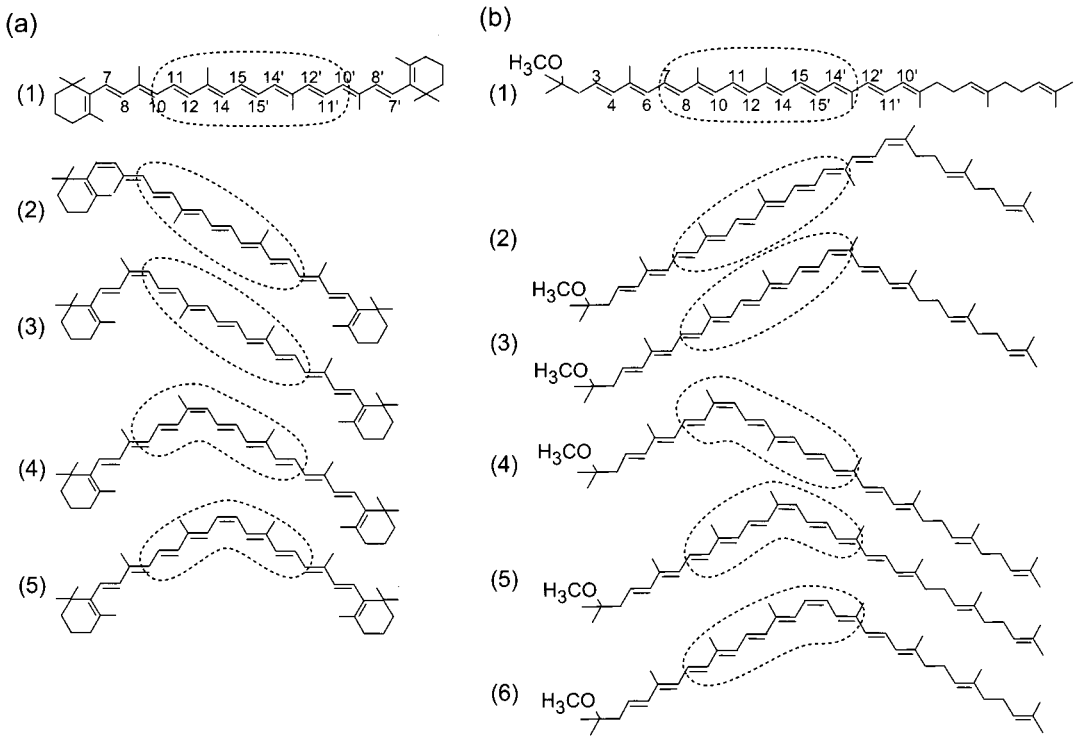

Figure 1. Configurations of (a) isomeric β-carotenes including the (1) all-trans, (2) 7-cis, (3) 9-cis, (4) 13-cis, and (5) 15-cis isomers and those of (b) isomeric spheroidenes including the (1) all-trans, (2) 9′-cis, (3) 13′-cis, (4) 9-cis, (5) 13-cis, and (6) 15-cis isomers. The triplet-excited regions are shown within the broken line.

tion spectra and decay time constants, whereas the 7-cis, 9-cis, and 13-cis isomers exhibited different spectral patterns and decay time constants of their own. The results suggested an extremely rapid cis-to-trans isomerization in the triplet state for the 15-cis isomer (the 15-cis T_1 was considered to be too short-lived to be detected). The quantum yields of triplet-sensitized isomerization were determined to be 15-cis (0.98), 13-cis (0.87), 9-cis (0.15), and 7-cis (0.12),[23] supporting the above idea.

In the present investigation, we have examined the triplet-state properties of a set of cis−trans isomers of spheroidene (shown in Figure 1b) by time-resolved absorption spectroscopy and by determination of the quantum yields of isomerization. It is interesting to compare the triplet-state properties of isomeric β-carotene (a symmetric carotenoid in algae[24] and higher plants[25]) to those of spheroidene (an asymmetric bacterial carotenoid[26]). Further, we have tried to determine the decay time constant and the rate of cis-to-trans isomerization of each cis T_1 species. In the analysis of the time-resolved spectra, we used singular-value decomposition and subsequent global fitting of the time-resolved spectra by the use of a scheme having potential minima at the cis and trans positions; we also used the quantum yields of isomerization determined by independent experiments. Our particular interest was whether we could detect, by time-resolved absorption spectroscopy, the process of isomerization from the cis T_1 to the all-trans T_1 upon triplet excitation using a sensitizer, anthracene. On the basis of the intrinsic T_1-state properties of isomeric spheroidenes in solution, we aimed to reexamine the hypothetical mechanism of triplet-energy dissipation by 15-*cis*-spheroidene in the RC from *Rb. sphaeroides*, which we proposed previously.[20,27−29]

Materials and Methods

Sample Preparation. All-trans-spheroidene was extracted from the cells of *Rb. sphaeroides* 2.4.1 and purified by the method described previously.[4,30] 9′-*cis*-Spheroidene, 13′-*cis*-spheroidene, 9-*cis*-spheroidene, and 13-*cis*-spheroidene were isolated by a combination of silica gel and calcium hydroxide column chromatography (to increase the purity of each isomer) from an isomeric mixture, which was obtained by iodine-sensitized photoisomerization of the all-trans isomer. The former chromatography used HPLC columns packed with Ultron VX-SIL 5 μm (Shinwa Chemical Co. Ltd, Kyoto) or Lichrosorb Si-60 5 μm (Merck) and an eluent, 0.8−2.3% diethyl ether in *n*-hexane containing 0.05% *N*,*N*-diisopropylethylamine. The latter chromatography, which was necessary to isolate the 13′-cis and 13-cis isomers, used columns packed with calcium hydroxide (Junsei Chemical Co. Ltd., lot 7H1232) and an eluent, 5.5% acetone in *n*-hexane (modified from the method of ref 4).

15-*cis*-Spheroidene was isolated from the RC of *Rb. sphaeroides* 2.4.1 as described previously.[4] For a large-scale preparation of the RC, the chromatophores were solubilized at 28 °C by stirring with 0.3% LDAO in 20 mM Tris-HCl (pH 8.0) containing 150 mM NaCl for 30 min. The supernatant after centrifugation (25 000*g*, 10 min) was dialyzed against 0.1% LDAO in 20 mM Tris-HCl (pH 8.0) and then passed through an ultrafiltration system (TOSOH, JSK model SC-60 equipped with a UF-3000 PS filter). The RC component (the filtrate) was then purified by ammonium sulfate (2.27 M) precipitation.

The purity of each isomer was examined by HPLC analysis and then by ^{1}H NMR spectroscopy (digital resolution, 0.24 Hz) after the assignment of all the ^{1}H signals by the use of its COSY and ROESY spectra.

Determination of the Molar Extinction Coefficients. Electronic absorption spectra of isomeric spheroidenes were recorded on a Hitachi U-2000 spectrophotometer. The molar extinction coefficient (ϵ) of each isomer was determined in *n*-hexane solution, in reference to that of the all-trans isomer, 173 600 M^{-1} cm^{-1},[31] by scaling electronic absorption spectra

of a pair of isomeric mixtures that were equilibrated by iodine-sensitized photoisomerization starting from the cis isomer in question and the all-trans isomer for reference. In the equilibration, a mixture of $\sim 4 \times 10^{-6}$ M spheroidene and 8×10^{-8} M I_2 was irradiated for 20 min at room temperature with a 15 W fluorescence lamp from a distance of 20 cm. The silica gel HPLC analysis confirmed the generation of mixtures with very similar isomeric compositions (practically no decomposition of the carotenoid was observed). The relative extinction coefficient was determined for each pair of samples by averaging the values of three independent measurements. The purity of each sample used in the determination of ϵ was as follows: all-trans, 99%; 9′-cis, 99%; 13′-cis, 99%; 9-cis, 95%; 13-cis, 97%; 15-cis, 98%.

Determination of the Quantum Yields of Triplet-Sensitized Isomerization. The quantum yield of triplet-sensitized isomerization (as defined by decrease in the starting isomer per triplet species generated) was determined for each isomer in *n*-hexane solution containing 5×10^{-5} M isomeric spheroidene and 5×10^{-5} M anthracene. The sample solution was irradiated with the 355 nm pulses (power, 1.0−1.2 mJ/pulse; duration, 12 ns; repetition rate, 2.5 Hz) from a Nd:YAG laser (Lumonics HY-400); the amount of isomerization was limited to <20%. The number of photons supplied was determined by using a chemical actinometer, potassium ferrioxalate.[32,33] The number of photons absorbed by anthracene was calculated by the use of the ϵ value at 355 nm, 8605 M^{-1} cm^{-1}, which was estimated by the use of the ϵ value at 374 nm, 8492 M^{-1} cm^{-1}.[34] The number of triplet anthracene generated was then calculated by using the quantum yield of intersystem crossing, 0.75.[35] The efficiency of triplet-energy transfer from anthracene to all-trans-spheroidene, $\Phi_{ET} = 0.89$, was obtained in the present investigation by the use of the decay rate of 5×10^{-5} M anthracene in *n*-hexane, 1.29×10^5 s^{-1}, and the rate of anthracene-to-spheroidene triplet-energy transfer, $k_{ET} = 2.10 \times 10^{10}$ M^{-1} s^{-1}. The k_{ET} value was determined by a Stern−Volmer plot[36] of the decay rate of T_1 anthracene (5×10^{-5} M) as a function of the concentration of all-trans spheroidene (1, 2, 3.5, and 5×10^{-5} M). The same Φ_{ET} value was assumed for the cis isomers. The initial purity of each isomer in the quantum-yield determination was as follows: all-trans, 96%; 13′-cis, 9-cis, 13-cis, and 15-cis, ~100%.

Time-Resolved Absorption Spectroscopy. A *n*-hexane solution (20 mL) containing 3×10^{-5} M isomeric spheroidene and 3×10^{-4} M anthracene was bubbled with nitrogen gas (>99.999%) for 20 min and then circulated through a quartz flow cell (optical path length, 2 mm). In the measurements of time-resolved spectra in the 400−550 nm region, probing light from a Xe-flash lamp (Tokyo Instruments, Tokyo, XF-80, fwhm = 60 μs, 1 kV) was used to irradiate the sample in the flow cell; the transmitted light was passed through an L-37 sharp cut filter (HOYA, Tokyo) and led into a spectrometer (SpectraPro-275i, Acton, Massachusetts) equipped with a dual diode-array detector (DIDA-512G, Princeton Instruments, Trenton). The gate width of the detector was set to 50 ns. For pumping the sensitizer, anthracene, the 355 nm pulses from a Nd:YAG laser (Lumonics, Warwickshire, HY-400) (pulse duration, 10 ns; power, 2 mJ/pulse; repetition, 1 Hz) irradiated the flow cell from an angle of ~20° with respect to the probe light. Timing between the pump pulse and the gated probe pulse (100 ns) was adjusted electronically, and the interval of delay time in collecting time-resolved spectra was set to be 0.2 μs (−0.4 to 20 μs) or 0.4 μs (20−39 μs). Three shots of time-resolved spectra were accumulated at a single delay time, but no smoothing of the resultant spectrum was performed. The purity of sample in solution changed as follows during the measurement of a set of time-resolved spectra (a 20 mL circulating sample solution was irradiated with 150 pairs of pump and probe pulses in total): all-trans, 95% to 94%; 9′-cis, 98% to 98%; 13′-cis, 99% to 93%; 9-cis, 98% to 94%; 13-cis, 99% to 94%; and 15-cis, 99% to 93%.

Results

The Initial and the Final Ground-State Configurations. Figure 1b shows a set of cis−trans isomers of spheroidene studied in the present investigation. As mentioned in the Introduction section, spheroidene is an asymmetric carotenoid, of which the conjugated part is shifted to the left (in this figure) with respect to the center of the entire C_{40} skeleton. The cis isomers can be classified into three groups in terms of the location of the cis-bend structure in the conjugated chain: (i) the all-trans type isomers having the stretched all-trans conjugated chain, which include all-trans and 9′-cis; (ii) the peripheral-cis isomers having the cis bend in the peripheral, which include 13′-cis and 9-cis; (iii) the central-cis isomer having the cis bend in the center, which include 13-cis and 15-cis. (Hereafter, we will use, whenever convenient, this set of inclusive terms, the "all-trans type", "peripheral-cis" and "central-cis" isomers.) On the other hand, the 13′-cis, 9-cis, and 13-cis isomers are classified into methylated-cis isomers and the 15-cis isomer into an unmethylated-cis isomer.

Figure 2 shows a set of time-resolved spectra after anthracene-sensitized excitation of the isomeric spheroidenes to the T_1 state: the $T_n \leftarrow T_1$ absorption of anthracene appears in the blue side and that of spheroidene in the red side with vibrational structures. The bleaching of the $1B_u^+ \leftarrow$ ground ($1A_g^-$) absorptions (shown at the top) appears between them. In the case of the all-trans type isomers (panels 1 and 2), the time-resolved spectra show their excitation to the T_1 state and subsequent relaxation to the original ground-state isomer; all of the above profiles disappear at 39 μs almost completely. In the case of the central-cis isomers (panels 5 and 6), their excitation to the T_1 state and relaxation to the all-trans isomer are seen as a major component; the time-resolved spectra at 39 μs after excitation exhibit the S_0 state absorptions, which are slightly shifted to the red in comparison to that of pure all-trans isomer (see the spectrum at the top of panel 1). In the peripheral-cis isomers (panels 3 and 4), excitation to the T_1 state and subsequent relaxation into both the original and the all-trans isomers take place; as a result, a difference spectrum of the all-trans isomer minus the starting cis isomer is seen in each of them.

To spectroscopically identify the final products, we first tried to determine the electronic absorption spectra of the set of isomers, that is, the wavelengths of absorption peaks and the molar extinction coefficients. Figure 3 shows the spectral profiles of the set of isomers (the ordinate scale represents molar extinction coefficient). Table 1 lists the wavelengths and the molar extinction coefficients for the $1B_u^+ \leftarrow 1A_g^-$, $1A_g^+ \leftarrow 1A_g^-$, and $2B_u^+ \leftarrow 1A_g^-$ vibronic transitions, which we will hereafter call "the main peak", "the cis peak" and "the overtone", respectively. Close examination of the wavelengths and the intensities of the vibronic peaks leads us to a classification of the isomers into three groups, (i) all-trans and 9′-cis, (ii) 13′-cis and 9-cis, and (iii) 13-cis and 15-cis. This classification in terms of spectral profiles agrees with that in terms of the configuration of the conjugated chain mentioned above, (i) the all-trans type, (ii) the peripheral-cis, and (iii) the central-cis isomers. More specifically, the intensity of the main peak

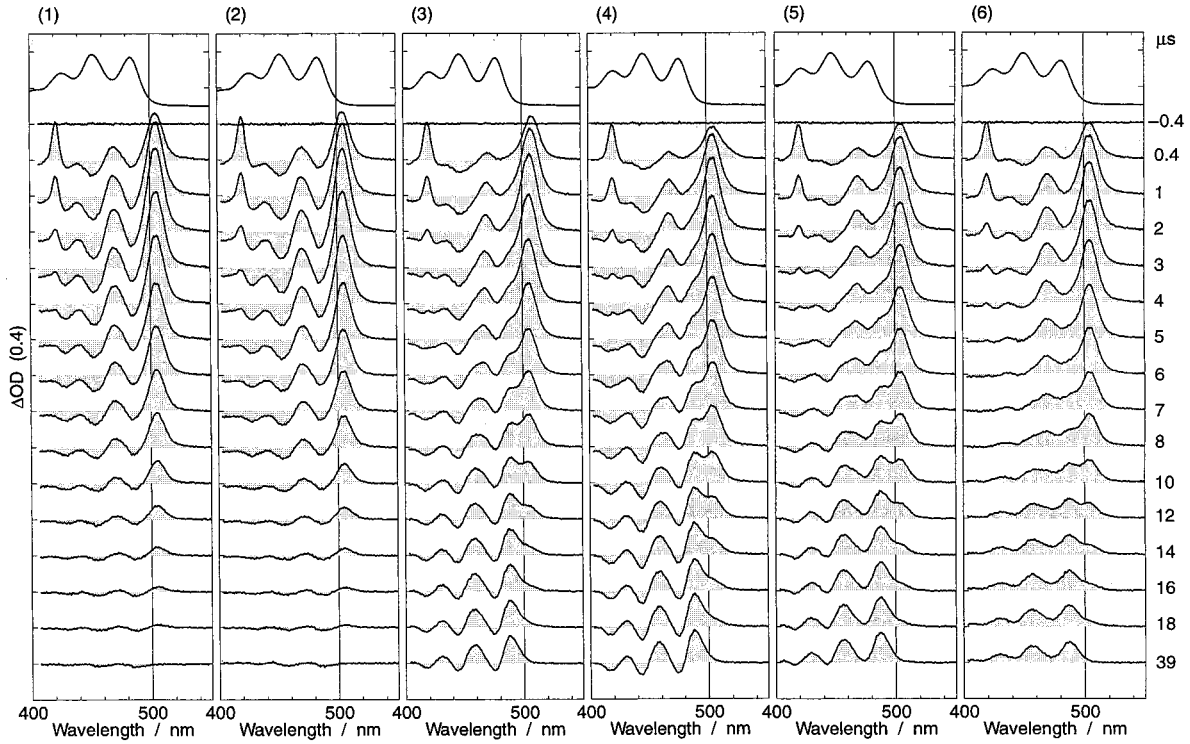

Figure 2. Time-resolved electronic absorption spectra of a mixture of each isomeric spheroidene (3×10^{-5} M) and anthracene (3×10^{-4} M) after excitation of anthracene at 355 nm: (1) all-trans; (2) 9′-cis; (3) 13′-cis; (4) 9-cis; (5) 13-cis; (6) 15-cis isomers. Normalized, ground (S_0)-state absorption spectra are also shown for comparison on the top of each set of time-resolved spectra.

TABLE 1: The Wavelengths of Vibronic Transitions (nm) and the Molar Extinction Coefficients ($\times 10^{-5}$ M^{-1} cm^{-1}) of the Main Peak, the cis Peak, and the Overtone Peak for the All-trans and Mono-cis Isomers of Spheroidene

	overtone			cis peak			main peak					
mono cis isomer	1 ← 0	0 ← 0	ϵ_{max}	1 ← 0	0 ← 0	ϵ_{max}	3 ← 0	2 ← 0	1 ← 0	0 ← 0	ϵ_{max}	ϵ_{450nm}
all-trans	268	279	0.363	331	345	0.171	404	426	453	484	1.736	1.675
9′-cis	269	279	0.329	331	346	0.162	404	427	453	484	1.729	1.660
13′-cis	270	281	0.187	331	345	0.481	400	423	448	477	1.477	1.418
9-cis	270	281	0.312	332	346	0.327	399	422	447	477	1.484	1.383
13-cis	272	283	0.219	331	345	0.728	399	422	448	478	1.241	1.191
15-cis	272	281	0.203	333	347	0.671	402	425	451	482	1.236	1.236

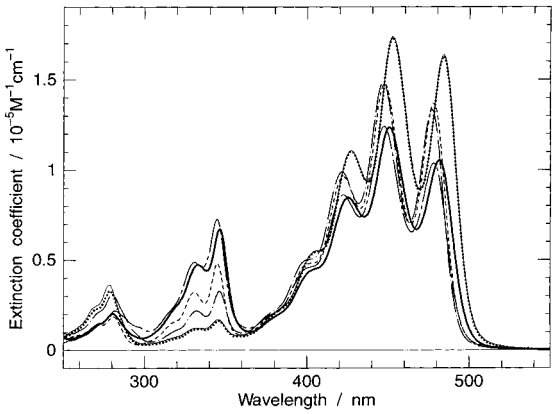

Figure 3. Ground (S_0)-state electronic absorption spectra of isomeric spheroidenes: all-trans (−); 9′-cis (···), 13′-cis (− − −), 9-cis (− · −), 13-cis (− - −) and 15-cis (—) isomers. See Table 1 for the wavelengths of vibronic transitions and the molar extinction coefficients.

decreases, whereas that of the cis peak increases in the following order: all-trans ≈ 9′-cis, 13′-cis, 9-cis, and 13-cis. Because the transition moment of the main peak is almost parallel, whereas that of the cis peak is perpendicular, to the long axis of the conjugated chain, the systematic changes in the intensities of those peaks can be easily understood.[37−39] On the other hand, the wavelength of the main peak (overtone) tends to shift to the blue (red) in this order, although the cis peak stays at approximately the same position. The 15-cis isomer does not necessarily follow the above trends. It is to be noted that the intensity of the cis peak relative to that of the main peak in the 13-cis isomer (0.59) is slightly higher than that in the 15-cis isomer (0.54), reflecting the central-cis nature of the former in reference to the conjugated chain. This result is contradictory to our previous report [15-cis (0.45), 13-cis (0.32) in ref 4]. The previous spectroscopic data for the 9′-cis and 13-cis isomers that were purified only by calcium hydroxide chromatography need to be revised; their purities were substantially lower than those of the present preparation using both the calcium hydroxide and silica gel chromatography.

Figure 4a compares, for each cis isomer, a difference spectrum of all-trans minus cis (shown in broken line) to the time-resolved spectrum at 39 μs after relaxation to the ground state (solid line). The difference spectrum was calculated by the use of the quantum yields of triplet-sensitized isomerization (see below) and the electronic absorption spectra of the pair of isomers determined above. The agreement between the observed and the calculated spectra establishes the overall isomerization process from each cis S_0 eventually to the all-trans S_0.

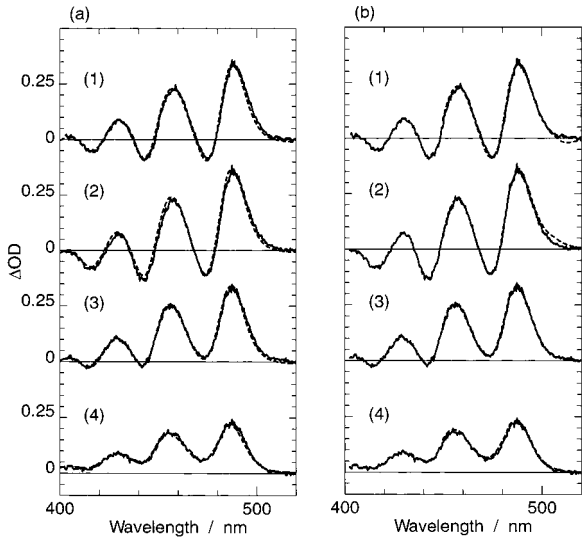

Figure 4. Comparison of the time-resolved absorption spectrum at 39 μs after excitation (solid line) with (a) a calculated difference spectrum of all-trans S_0 minus each cis S_0 by the use of the spectra in Figure 3 and the quantum yield of triplet-sensitized isomerization (broken line) and with (b) the species-associated difference spectrum (SADS) of the (trans−cis) S_0 component in the three-component analysis (broken line): (1) 13′-cis; (2) 9-cis; (3) 13-cis; (4) 15-cis isomers.

TABLE 2: Quantum Yields of Triplet-Sensitized Isomerization (Φ_{iso}) for Various Isomerization Pathways Starting from the All-trans and Mono-cis Isomers

	isomers produced					
starting isomers	all-trans	9′-cis	13′-cis	9-cis	13-cis	15-cis
all-trans		0.02	0.01	0.01	0.01	0.00
13′-cis	0.48	0.00		0.00	0.00	0.00
9-cis	0.50	0.00	0.00		0.00	0.00
13-cis	0.52	0.00	0.00	0.00		0.00
15-cis	0.60	0.00	0.00	0.00	0.00	

To determine the quantum yields of isomerization for different pathways starting from each cis or the all-trans isomer, we analyzed by HPLC the final products of the triplet-sensitized isomerization (see Table 2). Surprisingly, no cis-to-cis isomerization was identified at all in cis spheroidenes, a strong contrast to the case of cis-β-carotenes (see Table 3 of ref 23). Most importantly, the quantum yields of the cis-to-trans isomerization via the T_1 state (Φ_{iso}) have been determined to be 0.48, 0.50, 0.52, and 0.60 (error < 0.01) for the 13′-cis, 9-cis, 13-cis, and 15-cis isomers, respectively. The set of the Φ_{iso} values in the isomeric spheroidenes is between that of 7-*cis*- and 9-*cis*-β-carotene (0.12 and 0.15) and that of 13-*cis*- and 15-*cis*-β-carotene (0.87 and 0.98).

Cis-to-trans Isomerization in the T_1 State. (*a*) *A Preliminary Examination of the Time-Resolved Spectra.* Close examination of the time-resolved spectra shown in Figure 2 leads us to the identification of a time-dependent blue shift in the strongest $T_n \leftarrow T_1$ absorption of the 13′-cis and 9-cis isomers immediately after triplet excitation (panels 3 and 4). Figure 5 shows the shifts of the $T_n \leftarrow T_1$ absorption peak that were extracted by decomposition of the spectral profile in the longest wavelength side by the use of a pair of Gaussian peaks. The all-trans type isomers exhibiting no shifts at all are excluded from the figure. Most importantly, the $T_n \leftarrow T_1$ absorptions of the peripheral 13′-cis and 9-cis isomers exhibit shifts of approximately 3 and 1.5 nm, respectively. This observation strongly suggests the contribution of the cis T_1 species at an initial stage. The shifts are very small in the 13-cis and 15-cis isomers, suggesting one or both of the following two possibilities: (i) their shifts are too fast to be detected, although their $T_n \leftarrow T_1$ absorptions are actually red-shifted from that of the all-trans isomer; (ii) the wavelengths of their $T_n \leftarrow T_1$ absorptions are practically the same as that of the all-trans isomer.

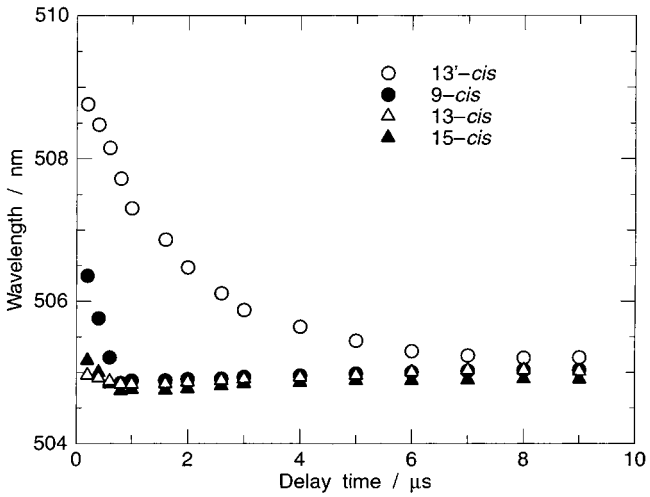

Figure 5. The shift of the $T_n \leftarrow T_1$ absorption maximum that was obtained by decomposition of the longest-wavelength profile of the time-resolved electronic absorption spectra by the use of a pair of Gaussian peaks: 13′-cis (○); 9-cis (●); 13-cis (△); 15-cis (▲) isomers.

(*b*) *Singular-Value Decomposition of the Time-Resolved Spectra.* Spectral analysis using singular-value decomposition (SVD) was performed for a data matrix of 513 wavelengths and 150 delay times. The details of the SVD and subsequent global-fitting procedure were described in ref 40 and references therein. Figure 6 shows the results of the SVD analyses of the time-resolved spectra for the 13′-cis, 9-cis, 13-cis, and 15-cis isomers, which include the singular values, V_i, the basis spectra, $\mathbf{s}_i$, and the temporal evolutions, $V_i\mathbf{t}_i$; for the latter two, only the three components having the largest V_i values (V_1, V_2, and V_3) are shown. The relative magnitudes of the V_i values, as well as the basis spectra and the time evolution for the first three components, are similar to one another among the four cis isomers, a fact which indicates that the time-dependent spectral changes reflect basically the same scheme of isomerization. When the basis spectra and the time evolutions are compared more closely among them, the following characterizations can be made. In the 13′-cis isomer, all of the first three components are very clear: the V_3 value is distinctly larger than the V_4 value; the *S*/*N* ratio of the $\mathbf{s}_3$ basis spectrum is comparable to those of $\mathbf{s}_1$ and $\mathbf{s}_2$; the $V_3\mathbf{t}_3$ time evolution exhibits a clear rise and decay immediately after excitation. In the 9-cis isomer, the third component is less clear: the V_3 value is considerably smaller, the *S*/*N* ratio of the $\mathbf{s}_3$ basis spectrum is lower, and the rise of the $V_3\mathbf{t}_3$ time evolution is less clear. In the 13-cis and 15-cis isomers, the V_3 value is almost comparable to the V_4 value, the $\mathbf{s}_3$ basis spectrum is noisy, and the rise and decay of the $V_3\mathbf{t}_3$ time evolution is hardly recognizable. The set of observations for the central-cis isomers corresponds to that of the tiny blue shifts of the strongest $T_n \leftarrow T_1$ absorption extracted from the real time-resolved spectra (see Figure 5).

The above characterizations lead us to the following conclusions: (i) A two-component analysis, including only the all-trans T_1 species and the result of cis-to-trans isomerization via the T_1 state [hereafter we abbreviate this "(trans−cis) S_0"], is applicable to the central 13-cis and 15-cis isomers as an approximate analysis. (ii) A three-component analysis, including the cis T_1 and the all-trans T_1 species as well as the (trans−cis)

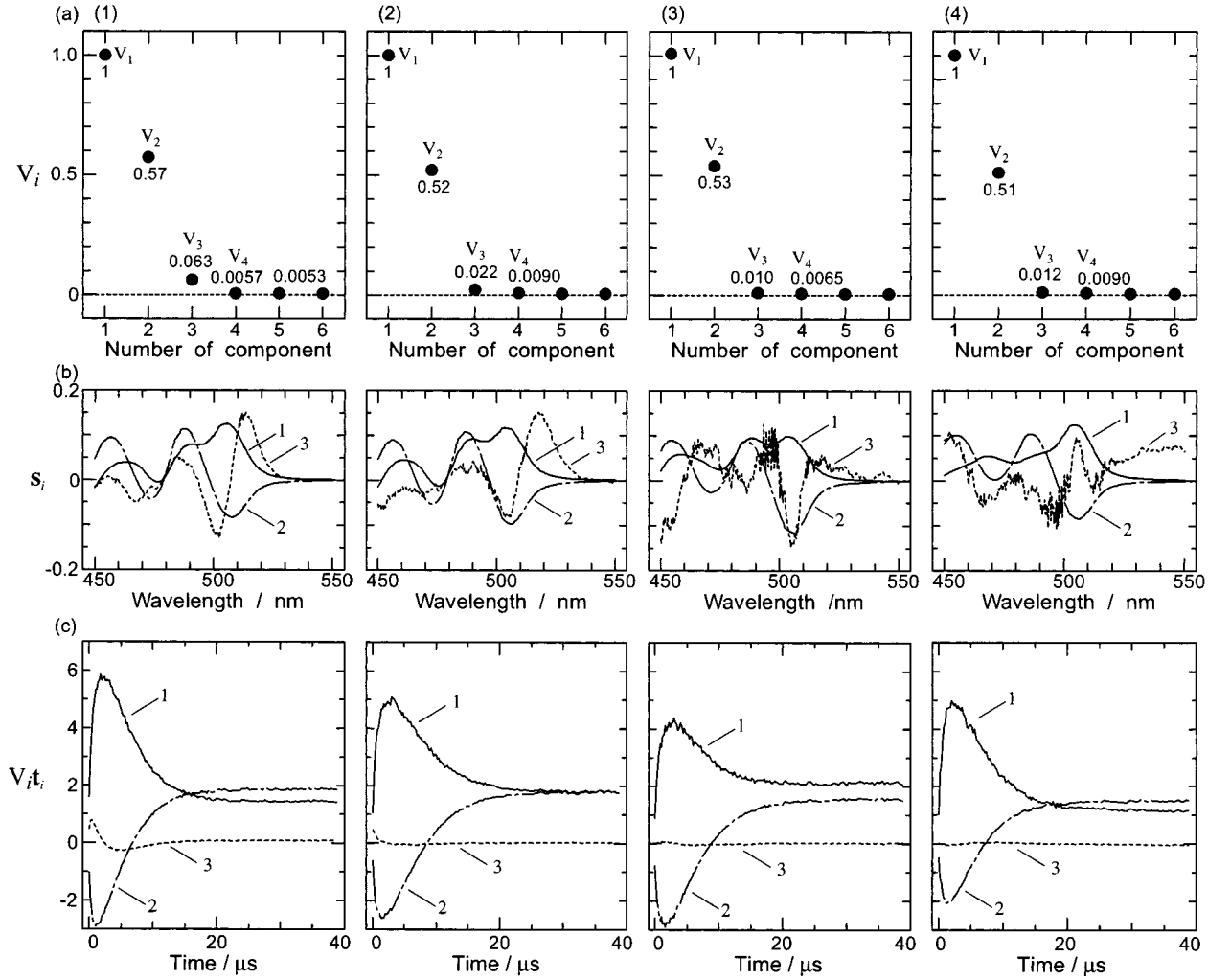

Figure 6. The results of singular-value decomposition (SVD) of the time-resolved electronic absorption spectra, including (a) the singular values, V_i, (b) the basis spectra, $\mathbf{s}_i$, and (c) the temporal evolutions, $V_i\mathbf{t}_i$, for the major three components: (1) 13′-cis; (2) 9-cis; (3) 13-cis; (4) 15-cis isomers.

S_0 component, should definitely be applied to the peripheral 13′-cis and 9-cis isomers, although its application to the central 13-cis and 15-cis isomers may not be straightforward.

(*c*) *Global Fitting of the Time-Resolved Spectra using Schemes 1 and 2*. We first tried to derive an equation that describes the triplet-energy transfer from anthracene (the sensitizer) to each isomeric spheroidene. Then, the excited-state dynamics of isomeric spheroidene can be described as a convolution of this equation, which plays the role like an instrumental response function (IRF), and the integrated population function, which will be described later.

In the present investigation, spheroidene was excited to the T_1 state through triplet-energy transfer from T_1-state anthracene,

$$\text{ant.}^{T_1} + \text{car.}^{S_0} \xrightarrow{k_{ET}} \text{ant.}^{S_0} + \text{car.}^{T_1} \tag{1}$$

However, at the present concentration of anthracene (3×10^{-4} M), we observed that triplet−triplet annihilation reaction took place between a pair of T_1 anthracene molecules in addition to its intrinsic decay,

$$\text{ant.}^{T_1} + \text{ant.}^{T_1} \xrightarrow{k_{ann}} 2\text{ant.}^{S_0} \tag{2}$$

$$\text{ant.}^{T_1} \xrightarrow{k_D} \text{ant.}^{S_0} \tag{3}$$

These reactions lead us to a rate equation,

$$\frac{dn_{ant.}^{T_1}}{dt} = -k_{ET} n_{car.}^{S_0} n_{ant.}^{T_1} - k_{ann}(n_{ant.}^{T_1})^2 - k_D n_{ant.}^{T_1} \tag{4}$$

When change in $n_{car.}^{S_0}$ is neglected, it becomes Bernoulli's differential equation. Then, it can be integrated as

$$n_{ant.}^{T_1} = \frac{n_0}{e^{K_2 t} + \left(\frac{K_1}{K_2} - 1\right)(e^{K_2 t} - 1)} \tag{5}$$

where

$$K_1 = \left(1 + \frac{k_{ann} n_0}{k_D + k_{ET} n_{car.}^{S_0}}\right)(k_D + k_{ET} n_{car.}^{S_0})$$

$$K_2 = k_D + k_{ET} n_{car.}^{S_0}$$

Here, n_0 is the number of anthracene molecules initially excited by the pumping pulse. Actually, the following equation was used as an approximation of eq 5:

$$n_{ant.}^{T_1} = n_0[C\, e^{-K_1 t} + (1 - C)\, e^{-K_2 t}] \tag{6}$$

Then, $k_{ET} n_{car.}^{S_0} n_{ant.}^{T_1}$ could be used as an IRF as defined above.

SCHEME 1

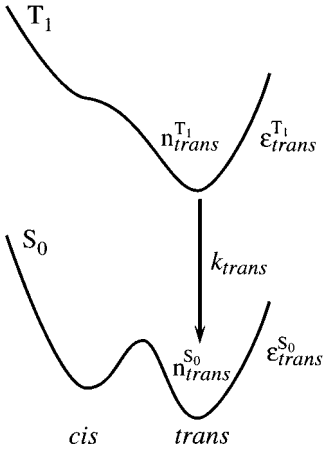

$$(\varepsilon^{T_1}_{trans} - \varepsilon^{S_0}_{cis})\, n^{T_1}_{trans} + (\varepsilon^{S_0}_{trans} - \varepsilon^{S_0}_{cis})\, n^{S_0}_{trans}$$

SCHEME 2

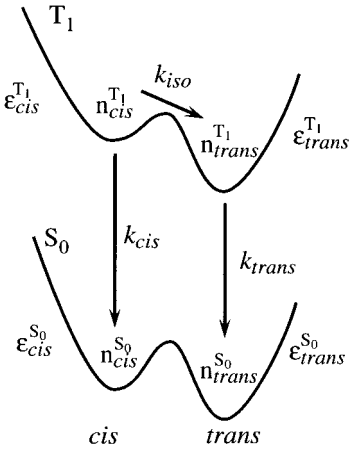

$$(\varepsilon^{T_1}_{cis} - \varepsilon^{S_0}_{cis})\, n^{T_1}_{cis} + (\varepsilon^{S_0}_{trans} - \varepsilon^{S_0}_{cis})\, n^{S_0}_{trans} + (\varepsilon^{T_1}_{trans} - \varepsilon^{S_0}_{cis})\, n^{T_1}_{trans}$$

Upon anthracene-sensitized triplet excitation, each cis or all-trans spheroidene molecule is supposed to be first deposited on the cis or the trans T_1 potential minimum, after dissipating the excess energy transferred from T_1 anthracene. Then, the pair of schemes, Schemes 1 and 2, could be used in the two-component and the three-component analyses, respectively.

In Scheme 1, the T_1-state cis-to-trans isomerization is supposed to be extremely rapid due to a shallow potential barrier between each cis and trans positions, and only the decay of the all-trans T_1 and the rise of the resultant all-trans S_0 are to be seen. The rate equations,

$$\frac{dn^{T_1}_{trans}}{dt} = -k_{trans} n^{T_1}_{trans} \tag{7}$$

$$\frac{dn^{S_0}_{trans}}{dt} = k_{trans} n^{T_1}_{trans} \tag{8}$$

lead us to a pair of integrated population functions,

$$n^{T_1}_{trans} = \Phi_{iso}\, e^{-k_{trans}t} \tag{9}$$

$$n^{S_0}_{trans} = \Phi_{iso}(1 - e^{-k_{trans}t}) \tag{10}$$

Here, Φ_{iso} represents the quantum yield of triplet-state isomerization effectively introduced.

In Scheme 2, the barrier between the cis and trans minima in the T_1 potential is supposed to be high enough to stabilize the cis T_1 species and to slow the isomerization to the all-trans T_1. Then, a set of rate equations,

$$\frac{dn^{T_1}_{cis}}{dt} = -(k_{cis} + k_{iso}) n^{T_1}_{cis} \tag{11}$$

$$\frac{dn^{T_1}_{trans}}{dt} = k_{iso} n^{T_1}_{cis} - k_{trans} n^{T_1}_{trans} \tag{12}$$

$$\frac{dn^{S_0}_{trans}}{dt} = k_{trans} n^{T_1}_{trans} \tag{13}$$

leads us to the integrated population functions,

$$n^{T_1}_{cis} = e^{-(k_{cis}+k_{iso})t} \tag{14}$$

$$n^{T_1}_{trans} = \frac{k_{iso}}{k_{trans} - (k_{cis} + k_{iso})} e^{-(k_{cis}+k_{iso})t} - \frac{k_{iso}}{k_{trans} - (k_{cis} + k_{iso})} e^{-k_{trans}t} \tag{15}$$

$$n^{S_0}_{trans} = \frac{-k_{iso}k_{trans}}{(k_{cis} + k_{iso})\{k_{trans} - (k_{cis} + k_{iso})\}} e^{-(k_{cis}+k_{iso})t} + \frac{k_{iso}}{k_{trans} - (k_{cis} + k_{iso})} e^{-k_{trans}t} + \frac{k_{iso}}{k_{cis} + k_{iso}} \tag{16}$$

Here, the quantum yield of triplet-state isomerization is given as

$$\Phi_{iso} = \frac{k_{iso}}{k_{cis} + k_{iso}} \tag{17}$$

The global-fitting procedure was performed to determine the coefficient matrix (hereafter, called "the **C** matrix") to fit the equation

$$V_i t_i^{\beta} = \sum_{j=1}^{p} C_{ij} n'_j(t^{\beta}), \quad i = 1, ..., p \tag{18}$$

where t^{β} stands for the delay times and $n'_j(t)$ ($i = 1, ..., p$) represents the population of each component. Then, the species-associated difference spectra (SADS) can be obtained by

$$(\mathrm{SADS})_j = \sum_{i=1}^{p} s_i C_{ij} \tag{19}$$

In the practical fitting, a convolution of the IRF (eq 6) and the set of integrated population functions of eqs 9 and 10 in Scheme 1 or eqs 14−16 in Scheme 2 was used as $n'_j(t)$.

The following strategy was used in the global-fitting procedure: (1) Time zero was fixed as experimentally determined. (2) The parameters in the IRF, K_1, K_2, and C in eq 6, were

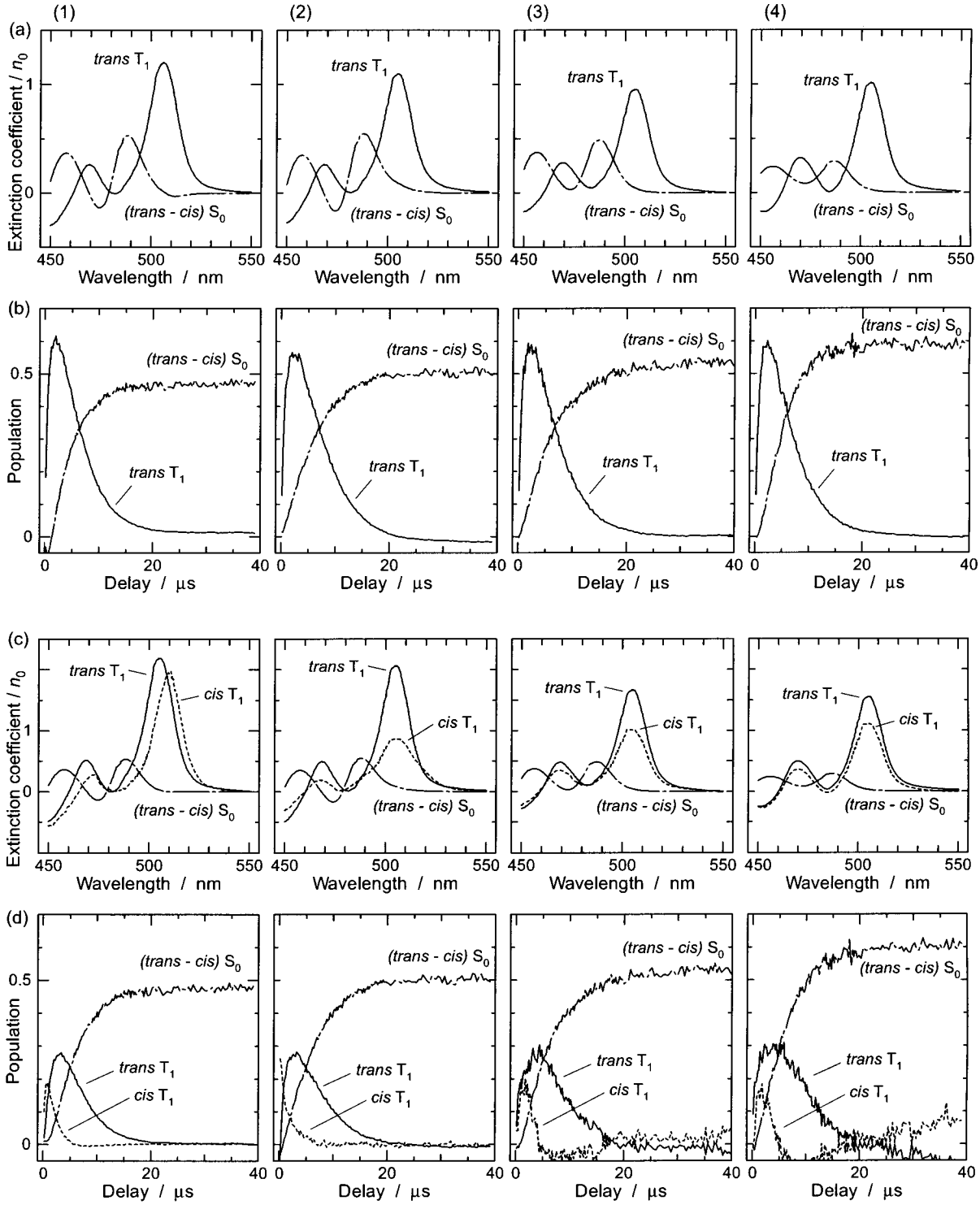

Figure 7. The results of global-fitting of the time-resolved electronic absorption spectra by the two-component analysis using Scheme 1 and the three-component analysis using Scheme 2 showing (a) the SADS and (b) the time profiles in the two-component analysis and (c) the SADS and (d) the time profiles in the three-component analysis: (1) 13′-cis; (2) 9-cis; (3) 13-cis; (4) 15-cis isomers.

fixed as determined in an experiment using 3×10^{-4} M anthracene and 3×10^{-5} M all-trans-spheroidene, where a manual decomposition of the $T_n \leftarrow T_1$ absorption of anthracene and the bleaching of the $1B_u^+ \leftarrow 1A_g^-$ absorption of spheroidene was performed. (3) The decay rate of the all-trans T_1 (k_{trans}) was fixed to an average of that for the all-trans isomer and those determined by the two-component analyses in the 13-cis and 15-cis isomers. (4) The quantum yields of isomerization (Φ_{iso}) that were determined by independent experiments were used to apply a constraint between the decay rate of the cis T_1 (k_{cis}) and the rate of isomerization (k_{iso}) (see eq 17). Then, the k_{cis} value and the **C** matrix were adjusted alternately by the least-squares method, the least-squares fitting being started from a first guess of k_{cis}. The **C** matrix and the rate constant eventually obtained were used to display the SADS and the time profile of each component shown in Figure 7.

Excited-State Dynamics of Isomeric Spheroidenes as Revealed by the SVD and Global Fitting Analyses. Sets of panels a and b in Figure 7 show the SADS and the time-dependent change in population (time profiles) for each isomer

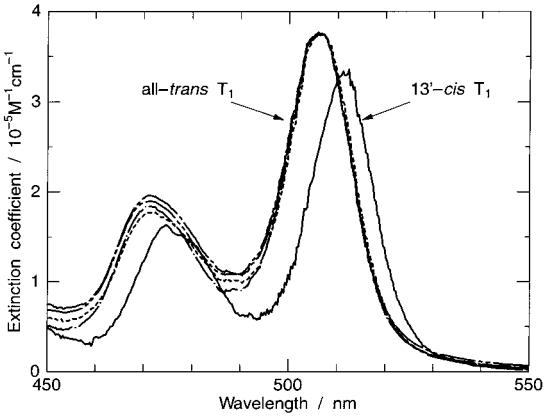

Figure 8. Comparison of the $T_n \leftarrow T_1$ absorptions of the all-trans T_1 generated from different cis isomers after compensating the contribution of bleaching of the S_0 absorption spectrum of the starting cis isomer: 13′-cis (− − −); 9-cis (− · −); 13-cis (− - −) and 15-cis (− - -). The $T_n \leftarrow T_1$ absorption spectrum of the 13′-cis T_1 (−) is also shown for comparison.

obtained by the two-component analysis using Scheme 1. The first component indicates the all-trans T_1 species generated from each cis T_1 as a result of the rapid cis-to-trans isomerization in the T_1 state. The second component indicates the (trans−cis) S_0 component generated by relaxation of the resultant all-trans T_1 to the S_0 state, or in other words, by isomerization from the starting isomer eventually to the all-trans isomer. The set of isomers gives rise to similar SADS and time profiles; differences originate from different quantum yields of T_1-state isomerization, which are reflected in the final population of (trans−cis) S_0. This two-component analysis is of limited value because the contribution of the cis T_1 species is completely neglected.

Sets of panels c and d in Figure 7 show the SADS and the time profiles obtained by the three-component analysis using Scheme 2. The SADS of temporally the first and the second components show the $T_n \leftarrow T_1$ absorptions of the cis T_1 and the all-trans T_1 species, respectively. The SADS of the third component shows the result of the overall cis-to-trans isomerization, (trans−cis) S_0. The set of time profiles shows the sequential transformations from the cis T_1 to the all-trans T_1 and eventually to the all-trans S_0. The three-component analysis is successful for the 13′-cis and the 9-cis isomers. However, it may not be too reliable in the 13-cis and 15-cis isomers because the time profiles of the cis T_1 species look a little strange in those central-cis isomers.

To test the reliability of the above results further, we examined the spectral patterns of the all-trans T_1 and the (trans−cis) S_0 for the set of cis isomers. Figure 8 compares the $T_n \leftarrow T_1$ absorption of the all-trans T_1 species generated from different cis isomers after compensation of the bleaching of the ground-state absorptions. The agreement in the spectral pattern is not complete but is acceptable, a support for the reliability of the present three-component analysis. Figure 4b compares for each isomer the SADS of the third component (broken line), (trans−cis) S_0, with the observed time-resolved spectrum at 39 μs after excitation (solid line). The excellent agreement constitutes another support for the reliability of this analysis. On the basis of the above results, we conclude that the present three-component analyses are reliable enough to use their results for discussion.

The results are summarized in Table 3, which lists the $T_n \leftarrow T_1$ absorption maxima and the rates of $T_1 \rightarrow S_0$ intersystem crossing for the all-trans T_1 and the cis T_1 species, and the rates of cis-to-trans isomerization for the four cis T_1 species. Figure 8 exhibits the $T_n \leftarrow T_1$ absorption of the 13′- cis T_1 species, which has been determined with the highest reliability.

TABLE 3: The $T_n \leftarrow T_1$ Absorption Maxima, the Rate of $T_1 \rightarrow S_0$ Intersystem Crossing (k_{trans} or k_{cis}), and the Rate of cis-to-trans Isomerization for the All-trans T_1 and cis T_1 Species

T_1 species	absorption (nm)	k_{trans} or k_{cis} ($\times 10^{-6}$ s^{-1})	k_{trans}^{-1} or k_{cis}^{-1} (μs)	k_{iso} ($\times 10^{-6}s^{-1}$)	k_{iso}^{-1} (μs)
all-trans	505	0.21	4.76		
13′-cis	510	1.2	0.83	1.1	0.91
9-cis	506	1.2	0.83	1.2	0.83
13-cis	505	1.2	0.83	1.3	0.77
15-cis	505	1.2	0.83	1.8	0.56

Discussion

Fast cis-to-trans Isomerization in the T_1 State and Time-Dependent Shift of the $T_n \leftarrow T_1$ Absorption as Explained in Terms of "the Triplet-Excited Region". "The triplet-excited region" has been defined, in carotenoids and retinoids, as a region of the conjugated chain where large changes in bond order take place upon triplet excitation; double bonds become more single-bond-like, whereas single bonds become more double-bond-like. It is localized in the central part of the conjugated chain, it has a span of five to six conjugated double bonds, and it triggers cis to trans isomerization in the T_1 state.[28] This concept is based on (1) theoretical and spectroscopic determination of the carbon−carbon bond orders in the all-trans isomers and (2) determination of the quantum yields of cis-to-trans isomerization via the T_1 state (see ref 20 for a review).

A Pariser−Parr−Pople calculation including singly and doubly excited configurational interactions for a model polyene of all-trans-β-carotene having 11 conjugated double bonds[23] as well as the determination of the C═C and C−C stretching force constants in the S_0 and T_1 states by means of normal-coordinate analysis of the S_0 and T_1 Raman spectra of variously deuterated all-trans-β-carotenes[41] showed decreases in the bond order of the C═C bond upon triplet excitation, of which the magnitude increased systematically from both peripherals to the center of the conjugated chain. As mentioned in the Introduction section, the quantum yield of triplet-sensitized isomerization increases in the order 7-cis (0.12), 9-cis (0.15), 13-cis (0.87), and 15-cis (0.98).[23] Therefore, the increasing quantum yield of isomerization from the peripheral-cis to the central-cis isomer can be explained in terms of the elongation of the C═C bond, upon triplet excitation, in the order from the peripheral to the center of the conjugated chain. When one assumes a triplet-excited region in the central part consisting of five double bonds and six single bonds in this particular carotenoid (see Figure 1a), the cis double bond is located out of this region in the 7-cis and 9-cis isomers, whereas it is in the middle of the region in the 13-cis and 15-cis isomers. Thus, the large difference in the quantum yield between the peripheral-cis and the central-cis isomers can be nicely explained.

Very recently, a set of stretching force constants reflecting bond orders has also been obtained in all-trans spheroidene.[41] Interestingly, the S_0-state C═C bond order decreases, from both peripherals to the center, symmetrically with respect to the 15═15′ bond (i.e., the center of the entire carbon skeleton), whereas the T_1-state C═C bond order decreases symmetrically with respect to the 13═14 bond, instead (i.e., the center of the conjugated chain). Based on this result, we assume, for this carotenoid, the triplet-excited region consisting of six double bonds and five single bonds in the central part of the conjugated

chain as shown in Figure 1b. Then, the cis bend sits at one end of the triplet-excited region in the 13′-cis isomer, and it shifts toward the center of the triplet-excited region in the order 9-cis, 15-cis, and then 13-cis. Thus, the systematic increase in the quantum yield of T_1-state isomerization (see Table 2) in the order 13′-cis (0.48), 9-cis (0.50), and 13-cis (0.52) can be explained. Accordingly, the rate of cis-to-trans isomerization (k_{iso}) increases systematically (see Table 3) in the order 13′-cis (1.1×10^6 s^{-1}), 9-cis (1.2×10^6 s^{-1}), and 13-cis (1.3×10^6 s^{-1}). It is interesting that the quantum yield (0.60) and the rate of isomerization (1.8×10^6 s^{-1}) are the highest for the 15-cis isomer, although the 13-cis isomer, instead, has the cis double bond in the most central part of the conjugated chain. The unmethylated-cis structure in the 15-cis isomer may be one of the factors that enhance the quantum yield of isomerization. The fast isomerization from either 15-cis or 13-cis to all-trans turns out to be one of the reasons that their T_1 species were difficult to detect by time-resolved absorption spectroscopy.

The shift of the $T_n \leftarrow T_1$ absorption peak of the cis T_1 species (in reference to that of the all-trans T_1) can also be speculatively explained in terms of the triplet-excited region. Table 3 shows that the shift decreases from the peripheral-cis to the central-cis isomer in the order 13′-cis (5 nm), 9-cis (1 nm), and 13-cis and 15-cis (0 nm). As mentioned above, the central C═C bonds are expected to be elongated upon triplet excitation, whereas the peripheral C═C bonds are left unchanged (as an intrinsic property of the triplet-excited region). Further, the introduction of a cis bend can also cause the elongation of the relevant double bond due to severe steric interaction in the concave side. Therefore, the cis bend can be easily accommodated within the central part of the triplet-excited region in the central-cis (13-cis and 15-cis) isomers, whereas it can be accommodated only after expanding the peripheral C═C bond in the peripheral-cis (13′-cis and 9-cis) isomers. In the latter case, the expansion of the peripheral C═C bond may cause a change in the T_1-state electronic structure, and as a result, the red shift of the $T_n \leftarrow T_1$ absorption band may take place.

Most importantly, the reasons for the difficulty in detecting the 15-cis T_1 and 13-cis T_1 species by time-resolved absorption spectroscopy of the present carotenoid are now explained; the difficulty originates from both their shorter T_1 lifetimes (vide supra) and their negligible shifts of the $T_n \leftarrow T_1$ absorption in reference to the lifetime and the absorption of the all-trans T_1.

A Possible Reason for the Selection of the 15-cis Configuration by the RC: The Fast Process of $T_1 \rightarrow S_0$ Intersystem Crossing Accompanying Efficient Dissipation of the Triplet Energy. In a previous investigation, we have proposed a hypothetical mechanism of triplet-energy dissipation by the RC-bound 15-cis car.[29] The proposal was based on the following experimental results: (1) extremely rapid isomerization from the 15-cis T_1 to the all-trans T_1 that was found in β-carotene by time-resolved Raman[21] and electronic absorption[22] spectroscopy and by determination of the quantum yields of triplet-sensitized isomerization[23] (see the Introduction section); (2) the substantially twisted and slightly twisted 15-cis configuration of the RC-bound spheroidene in the T_1 and S_0 states that were probed by transient and stationary-state Raman spectroscopy;[29] (3) the formation of 15-*cis*-spheroidene upon incorporation of all-trans-spheroidene into a carotenoidless RC from *Rb. sphaeroides*.[42] The mechanism proposed was as follows (see Figure 5 of ref 29): When the RC-bound car. in a slightly twisted 15-cis configuration in the S_0 state is excited to the T_1 state, it isomerizes along the T_1 potential curve and reaches the minimum at a substantially twisted position. The car. relaxes (intersystem crosses) down to the S_0 state from the T_1 minimum and then isomerizes along the S_0 potential curve back to the original slightly twisted 15-cis configuration. The rotational motion or twisting around the 15═15′ bond was supposed to be advantageous in dissipating the triplet energy through the $T_1 \rightarrow S_0$ intersystem crossing because the mixing of the π and σ orbitals in a twisted configuration facilitates coupling between change in the orbital angular momentum and change in the spin angular momentum.

The present results concerning the intrinsic T_1-state properties of the isomers of the relevant bacterial carotenoid (spheroidene) in solution have provided us with a strong support for the above mechanism: It has been shown that the rate of the $T_1 \rightarrow S_0$ intersystem crossing of the cis T_1 species is 6 times larger than that of the all-trans T_1 (Table 3), a fact which shows that any cis isomer in the RC must be more advantageous than the all-trans isomer in dissipating the T_1 energy through the relaxation process. Further, the rate of cis-to-trans isomerization increases in the order 13′-cis < 9-cis < 13-cis < 15-cis. Thus, the 15-cis T_1 must decay most rapidly and, therefore, dissipate the T_1 energy most efficiently. The barrier between the 15-cis and the 15-trans minima is expected to be very small. Most importantly, the rate of isomerization (0.56 μs, see Table 3) is on the same order of magnitude as the rate of intersystem crossing (0.83 μs), indicating that the change in the orbital angular momentum through the rotational motion around the 15═15′ bond (a nuclear motion) can strongly couple the change in the spin angular momentum accompanied by the $T_1 \rightarrow S_0$ intersystem crossing (an electronic transition). Therefore, the usage of the 15-cis configuration is expected to be most advantageous in dissipating the triplet energy. This fast process of intersystem crossing should take place during the rotational motion before reaching the all-trans configuration or even within the 15-cis T_1 potential minimum.

Although the intrinsic T_1-state property of the 15-cis isomer of spheroidene seems to support the proposed mechanism, an important question is what is the real mechanism of triplet-energy dissipation when the car. is bound to the RC. Most importantly, the complete rotational motion from 15-cis to all-trans is prohibited by the binding pocket of the apopeptide. Transient Raman spectroscopy of the RC-bound spheroidene[29] showed a substantial twisting of the cis C15═C15′ bond in the T_1 state, and the formation of the all-trans isomer was also identified when the sample was irradiated for a long time. The results indicate that the 15-cis to all-trans isomerization in the T_1 state is the driving force of the structural changes. Very recently, we have performed normal-coordinate analysis of the S_0 and T_1 Raman spectra of variously deuterated spheroidenes that were incorporated into the RC from a carotenoidless mutant of this bacterium (*Rb. sphaeroides* R26). The results can be summarized as follows:[41] (1) Large changes in carbon−carbon stretching force constants (bond order) take place in the central part of the conjugated chain, proving the formation of the triplet-excited region. Actually, the set of the T_1-state carbon−carbon constants for the RC-bound spheroidene was similar to that of all-trans-spheroidene in solution. On the basis of a correlation between the carbon−carbon stretching force constant and the bond length, the lengthenings of the C13═C14, C11═C12, and C15═C15′ bonds were estimated to be 0.05, 0.04, and 0.02 Å, respectively. (2) Twisting of the conjugated chain was found to take place upon triplet excitation. The twisting around the C15═C15′ cis bond and the C13═C14 and C11═C12 trans bonds was estimated to be 45°, −30°, and 30°, respectively. On the other hand, the twisting around the C15═C15′ bond in

the S_0 state was estimated to be 30°. This unique T_1-state structure of the RC-bound spheroidene can be regarded as the result of balance between (1) the changes in bond lengths and the rotational motion toward all-trans (as an intrinsic T_1-state properties of 15-*cis*-spheroidene) and (2) the steric repulsion with the binding pocket of the apopeptide.

All of the above results lead us to a slightly modified mechanism of triplet-energy dissipation: The rotational motion around the C15═C15′, C13═C14 and C11═C12 bonds to reach the above equilibrium structure must cause very efficient intersystem crossing (we call this "a fast process of intersystem crossing"), because the time-dependent changes in the orbital angular momentum can couple with changes in spin angular momentum to enhance the $T_1 \rightarrow S_0$ intersystem crossing.

A very recent theoretical calculation (Nagae et al. unpublished) showed that twisting around the C═C and C−C bonds in the central part of a conjugated chain enhances the spin−orbit coupling in the $S_0 \leftrightarrow T_1$ transition. Therefore, a precise determination of the rotational angles in both the S_0 and T_1 states will provide us with an important piece of information concerning the spin−orbit coupling. However, the identification of the above structural changes in the RC-bound 15-*cis*-spheroidene immediately after excitation to the T_1 state (before reaching the twisted equilibrium structure) is most important to establish the present *dynamic* mechanism. Time-resolved Raman spectroscopy will give us definitive information.

Finally, we would like to make a comment on a question raised by Bautista et al.[43] concerning our previous hypothetical mechanism.[29] They showed that the spectral properties and the excited-state dynamics of locked-15,15′-*cis*-spheroidene ("locked 15-*cis*-spheroidene") that was incorporated into the RC from *Rb. sphaeroides* R26.1 (a carotenoidless mutant) were similar to those of (unlocked) 15-*cis*-spheroidene in the RC from the *Rb. sphaeroides* 2.4.1. They determined the triplet decay time constant (τ_d) for the former to be 7 ± 1 μs.[43] The reported τ_d values for the latter, to be compared, include 4−5 ,[16] and 5 ± 2, 6.5, 5−10, and 7.2 ± 1 μs in the abstract, text, Figure 3b, and Table 1 of ref 44. Thus, the latter value is still controversial and should be regarded as slightly smaller than or similar to the former value. Obviously, the time constants of triplet decay discussed here are *after* the locked and unlocked 15-*cis*-spheroidenes reach to their own equilibrium structure (we call this "a slow process of intersystem crossing"). There is a good chance that the locked spheroidene forms another type of twisted conformation due to the elongation of the central double bonds of the car. conjugated chain in the binding pocket of the apopeptide. If the twistings around the C11═C12 and the C13═C14 bonds (possibly with an additional double bond other than the C15═C15′ bond) can cause a similar magnitude of spin−orbit coupling, the decay lifetime may not be so different. Therefore, it is absolutely necessary to make a comparison between the locked and the unlocked spheroidenes concerning the fast process of intersystem crossing or, in other words, the initial decay of the triplet population, which presumably takes place in the submicrosecond or even shorter time scales.

Acknowledgment. The authors thank Dr. Hiromu Sugeta for supporting the analysis of time-resolved spectra at an early stage of this investigation. Financial supports from the Science Research Promotion Fund and from the Japan Society for the Promotion of Science are gratefully acknowledged. R.F. has been supported by a JSPS fellowship for Japanese junior scientists and a grant-in-aid from the Ministry of Education, Science, Sports and Culture, Japan (Grant No. 7725).

References and Notes

(1) Koyama, Y.; Fujii, R. In *The Photochemistry of Carotenoids*; Frank, H. A., Young, A. J., Britton, G., Cogdell, R. J., Eds.; Kluwer Academic Publishers: Dordrecht, Netherlands, 1999; Chapter 9.

(2) Koyama, Y.; Kanaji, M.; Shimamura, T. *Photochem. Photobiol.* **1988**, *48*, 107.

(3) Lutz, M.; Szponarski, W.; Berger, G.; Robert, B.; Neumann, J.-M. *Biochim. Biophys. Acta* **1987**, *894*, 423.

(4) Jiang, Y.-H.; Kurimoto, Y.; Shimamura, T.; Ko-chi, N.; Ohashi, N.; Mukai, Y.; Koyama, Y. *Biospectroscopy* **1996**, *2*, 47.

(5) Koyama, Y.; Takatsuka, I.; Kanaji, M.; Tomimoto, K.; Kito, M.; Shimamura, T.; Yamashita, J.; Saiki, K.; Tsukida, K. *Photochem. Photobiol.* **1990**, *51*, 119.

(6) Bialek-Bylka, G. E.; Tomo, T.; Satoh, K.; Koyama, Y. *FEBS Lett.* **1995**, *363*, 137.

(7) Bialek-Bylka, G. E.; Fujii, R.; Chen, C.-H.; Oh-oka, H.; Kamiesu, A.; Satoh, K.; Koike, H.; Koyama, Y. *Photosynth. Res.* **1998**, *58*, 135.

(8) Bialek-Bylka, G. E.; Hiyama, T.; Yumoto, K.; Koyama, Y. *Photosynth. Res.* **1996**, *49*, 245.

(9) Yeates, T. O.; Komiya H.; Chirino, A.; Rees, D. C.; Allen, J. P.; Feher, G. *Proc. Natl. Acad. Sci. U.S.A.* **1988**, *85*, 7993.

(10) Arnoux, B.; Gaucher, J.-F.; Ducruix, A.; Reiss-Husson, F. *Acta Crystallogr.* **1995**, *D51*, 368.

(11) McAuley, K. E.; Fyfe, P. K.; Ridge, J. P.; Cogdell, R. J.; Isaacs, N. W.; Jones, M. R. *Biochemistry* **2000**, *39*, 15032.

(12) Lancaster, C. R. D.; Michel, H. *J. Mol. Biol.* **1999**, *286*, 883.

(13) Jordan, P.; Fromme, P.; Witt, H. T.; Klukas, O.; Saenger, W.; Krauss, N. *Nature*, **2001**, *411*, 909.

(14) Šetlíková, E.; Ritter, S.; Hienerwadel, R.; Kopecký, J.; Komenda, J.; Welte, W.; Šetlík, I. *Photosynth. Res.* **1995**, *43*, 201.

(15) Yruela, I.; Tomás, R.; Sanjuán, M. L.; Torrado, E.; Aured, M.; Picorel, R. *Photochem. Photobiol.* **1998**, *68*, 729.

(16) Cogdell, R. J.; Monger, T. G.; Parson, W. W. *Biochim. Biophys. Acta* **1975**, *408*, 189.

(17) Monger, T. G.; Cogdell, R. J.; Parson, W. W. *Biochim. Biophys. Acta* **1976**, *449*, 136.

(18) Frank, H. A.; Violette, C. A. *Biochim. Biophys. Acta* **1989**, *976*, 222.

(19) Frank, H. A. In *The Photosynthetic Reaction Center*; Deisenhofer, J., Norris, J. R., Eds.; Academic Press: San Diego, CA, 1993; Vol. II, Chapter 9.

(20) Koyama, Y.; Mukai, Y. In *Biomolecular Spectroscopy, Part B*; Clark, R. J. H., Hester, R. E., Eds.; Wiley & Sons Ltd.: Chichester, U.K., 1993; Chapter 2.

(21) Hashimoto, H.; Koyama, Y. *J. Phys. Chem.* **1988**, *92*, 2101.

(22) Hashimoto, H.; Koyama, Y.; Ichimura, K.; Kobayashi, T. *Chem. Phys. Lett.* **1989**, *162*, 517.

(23) Kuki, M.; Koyama, Y.; Nagae, H. *J. Phys. Chem.* **1991**, *95*, 7171.

(24) Haugan, J. A.; Aakermann, T.; Liaaen-Jensen, S. *Carotenoids*; Birkhäuser Verlag: Basel, Switzerland, 1995; Vol. 1A, Chapter 7, example 2.

(25) Britton, G. *Carotenoids*; Birkhäuser Verlag: Basel, Switzerland, 1995; Vol. 1A, Chapter 7, example 1.

(26) Britton, G.; Riesen, R. *Carotenoids*; Birkhäuser Verlag: Basel, Switzerland, 1995; Vol. 1A, Chapter 7, example 3.

(27) Koyama, Y. In *Carotenoids: Chemistry and Biology*; Krinsky, N. I., Mathews-Roth, M. M., Taylor, R. F., Eds.; Plenum Press: New York, 1990; p 207.

(28) Koyama, Y.; Mukai, Y.; Kuki, M. *SPIE Laser Spectrosc. Biomol.* **1992**, *1921*, 191.

(29) Ohashi, N.; Ko-chi, N.; Kuki, M.; Shimamura, T.; Cogdell, R. J.; Koyama, Y. *Biospectroscopy* **1996**, *2*, 59.

(30) Kuki, M.; Nagae, H.; Cogdell, R. J.; Shimada, K.; Koyama, Y. *Photochem. Photobiol.* **1994**, *59*, 116.

(31) Zhang, J.-P.; Fujii, R.; Qian, P.; Inaba, T.; Mizoguchi, T.; Koyama, Y.; Onaka, K.; Watanabe, Y.; Nagae, H. *J. Phys. Chem. B* **2000**, *104*, 3683.

(32) Hatchard, C. G.; Parker, C. A. *Proc. R. Soc. London, Ser. A.* **1956**, *235*, 518.

(33) Bowman, W. D.; Demas. J. N. *J. Phys. Chem.* **1976**, *80*, 2434.

(34) Quast, H.; Schön, N. *Liebigs Ann. Chem.* **1984**, 133.

(35) Medinger, T.; Wilkinson, F. *Trans. Faraday Soc.* **1965**, *61*, 620.

(36) Connors, K. A. *Chemical Kinetics The Study of Reaction Rates in Solution*; VCH Publishers: New York, 1990; Chapter 4.

(37) Koyama, Y.; Takii, T.; Saiki, K.; Tsukida, K. *Photobiochem. Photobiophys.* **1983**, *5*, 139.

(38) Hu, Y.; Hashimoto, H.; Moine, G.; Hengartner, U.; Koyama, Y. *J. Chem. Soc., Perkin Trans. 2* **1997**, 2699.

(39) Fujii, R.; Chen, C.-H.; Mizoguchi, T.; Koyama, Y. *Spectrochim. Acta, Part A* **1998**, *54*, 727.

(40) Zhang, J.-P.; Inaba, T.; Watanabe, Y.; Koyama, Y. *Chem. Phys. Lett.* **2000**, *331*, 154.

(41) Mukai-Kuroda, Y.; Fujii, R.; Ko-chi, N.; Sashima, T.; Koyama, Y.; Abe, M.; Gebhard, R.; van der Hoef, I.; Lugtenburg, J. *J. Phys. Chem. A*, in press.

(42) Agalidis, I.; Lutz, M.; Reiss-Husson, F. *Biochim. Biophys. Acta* **1980**, *589*, 264.

(43) Bautista, J. A.; Chynwat, V.; Cua, A.; Jansen, F. J.; Lugtenburg, J.; Grosztola, D.; Wasielewski, M. R.; Frank, H. A. *Photosynth. Res*. **1998**, *55*, 49.

(44) Frank, H. A.; Chynwat, V.; Posteraro, A.; Hartwich, G.; Simonin, I.; Scheer, H. *Photochem. Photobiol.* **1996**, *64*, 823.